Closed-loop controlled vortex-airfoil interactions

M. M. Zhang, L. Cheng,[a] and Y. Zhou
Department of Mechanical Engineering, The Hong Kong Polytechnic University, Hung Hom, Kowloon, Hong Kong

(Received 20 July 2005; accepted 23 February 2006; published online 12 April 2006)

Closed-loop controlled interactions between an airfoil and impinging vortices were experimentally investigated. This work aims to minimize the fluctuating flow pressure (p) at the leading edge of the airfoil, which is a major source of the blade-vortex interaction noises commonly seen in rotorcrafts. Piezoceramic actuators were used to create a local surface perturbation near the leading edge of the airfoil in order to alter the airfoil-vortex interaction. Two closed-loop control schemes were investigated, which deployed p and the streamwise fluctuating flow velocity (u) as the feedback signal, respectively. As the control effect on p was measured using a fast response pressure transducer, the oncoming vortical flow was monitored using a particle image velocimetry and a hot wire. It was found that the control scheme based on the feedback signal u led to a pronounced impairment in the strength of oncoming vortices and meanwhile a maximum reduction in p by 39%, outperforming the control scheme based on the feedback signal p. Physics behind the observations is discussed. © *2006 American Institute of Physics*. [DOI: 10.1063/1.2189287]

I. INTRODUCTION

When a hard-surfaced body such as blade, foil, wedge, or fin is subjected to an oncoming vortical flow, the incident vortices may be distorted so rapidly that a sharp pressure rise is induced at the leading edge of the body. This pressure rise in turn causes the generation of an intense impulsive sound and subsequent radiation to the far field.[1–5] This kind of noise, referred to as the blade-vortex interaction (BVI) noise, is commonly seen in engineering rotorcrafts, e.g., helicopters, turbomachines, and fans. This noise can also cause an environmental concern and even directly jeopardize the competitiveness and even the usage of the industrial products such as hair driers, vacuum cleaners, computers, and telecom exchangers, which are associated with the rotorcrafts. Therefore, the control of the BVI noise has recently been given an increasing attention in the literature.

Passive control methods have been extensively employed to reduce the BVI noise. Typical examples include modified blade tip shapes,[6] the use of spoilers or vane wings,[7] and flight path management.[8,9] Requiring no external energy input, these methods change the dynamic behavior of the fluid-structure system via modifying its geometrical or physical parameters.

Active control techniques have also been explored in the past. Active control can be either an open- or closed-loop. Using an open-loop method, Brooks *et al.*[10] simultaneously pitched the four blades of a hingeless BO-105 rotor up to 1.2° through electrohydraulic actuators at 3, 4, and 5 times of the rotor rotational frequency and managed to obtain a 6 dB reduction in BVI noise. Jackin *et al.*[11] improved this technique, leading to the so-called individual blade control (IBC). IBC allowed the independent control of each blade of a helicopter with servohydraulic actuators, resulting in a reduction in the BVI noise by 12 dB. Chen *et al.*[12] used surface-bounded piezoceramic actuators or fiber composites to twist an airfoil, achieving a 10 dB reduction in the BVI noise. Straub *et al.*[13] applied piezoelectrically driven trailing edge flaps to all blades of a MD900 light utility helicopter. The tip vortices shed from a preceding blade were effectively disturbed by the flap oscillations so that the BVI noise dropped by 5 dB. Kaykayoğlu[14] changed interactions between upstream vortices and a downstream airfoil by oscillating the leading edge of the airfoil, which was activated by a variable-speed dc motor. The vortex strength and the BVI noise were effectively suppressed when the oscillation frequency of the leading edge coincided with the instability frequency of the vortex-airfoil system. Lee[15] employed a bleeding technique, by blowing or sucking air through the porous leading edge of an airfoil, to perturb vortex-airfoil interaction, yielding a 30% reduction in the BVI noise in the near field.

A closed-loop control relies on a feedback signal from the controlled system to generate control actions. Most previous investigations were conducted numerically on the closed-loop control of the BVI noise. See Ariyur and Krstić[16] and Swaminathan *et al.*[17] for examples. Recently, Cheng *et al.*[18] proposed a perturbation technique to control fluid-structure interactions, which proved to be very effective in altering the strength of vortices shed from a cylinder and subsequently the structural vibration.[18,19] Inspired by that success, the present work extends the perturbation technique for a new application, i.e., modifying the blade-vortex interaction and subsequently suppressing the BVI noise.

A variety of methods for producing two-dimensional upstream vortices have been discussed by Wilder and Telionis.[20] The simplest is to employ a cylinder to generate von Kármán vortices, whose interaction with a downstream blade may reflect the major characteristics of BVI.[21] This method has been used by a number of researchers[4,20,22] and is

[a]Telephone: 00852-27666769. Fax: 00852-23654703. Electronic mail: mmlcheng@polyu.edu.hk

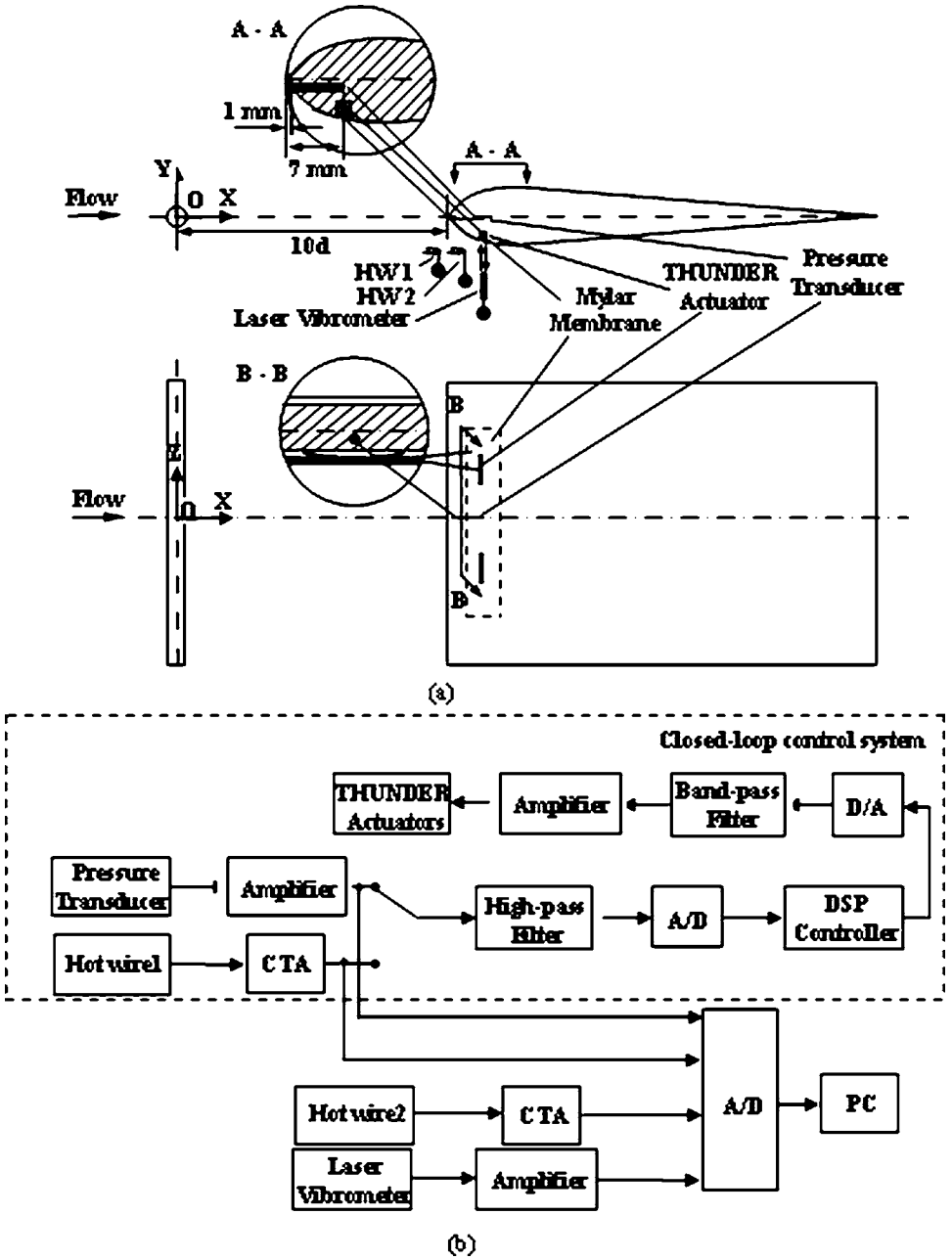

FIG. 1. Experimental setup: (a) Mechanical and sensing configuration and (b) schematic of closed-loop control system and measurement system.

adopted presently. The objective of this work is to develop a closed-loop control system and to effectively suppress the fluctuating flow pressure p at the airfoil leading edge in view of the fact that it is difficult to directly measure noise associated with fluid-structure interactions and that this pressure is responsible for the generation of the BVI noise.[4,15] Two closed-loop control schemes, using p and the streamwise fluctuating flow velocity u for feedback signals, respectively, were deployed and compared. The control performances were assessed in terms of p measured by a miniature pressure transducer. To understand the underlying physics, the control effects on the oncoming vortical flow were measured, simultaneously with p, using a hot wire and a particle image velocimetry (PIV), and the interactions between u, p and the perturbation were examined in detail.

II. EXPERIMENTAL DETAILS

Experiments were conducted in a closed circuit wind tunnel, which has a 2.4-m-long square test section of 0.6 m $\times$0.6 m. Readers may refer to Zhou *et al.*[23] for more details about the tunnel. A circular cylinder made of stainless steel with a diameter $d=10$ mm and an NACA0012 airfoil with a chord length $c=150$ mm and a thickness=18 mm were horizontally mounted in tandem on the test section (Fig. 1). The cylinder and the leading edge of the airfoil were separated by $10d$, which was sufficient to prevent significant flow feedback induced by the airfoil.[2] The airfoil angle of attack was set at 0°. Measurements were conducted at a free-stream velocity $U_\infty=11$ m/s. The corresponding Reynolds numbers, $\mathrm{Re}_d(\equiv U_\infty d/\nu$, where ν is the kinematic viscosity) based on d

and $\mathrm{Re}_c(\equiv U_\infty c/\nu)$ based on c were 7.3×10^3 and 1.09×10^5, respectively. The frequency f_s of vortex shedding from the cylinder was about 220 Hz. The free-stream turbulence intensity was less than 0.4%.

Two curved piezoceramic actuators, so called THUNDER, which were 76 mm long and 2.8 mm wide, were embedded in a slot of 200 mm long, 3 mm wide, and 3 mm deep on the lower side of airfoil, which was 7 mm from the airfoil leading edge in the streamwise direction [Fig. 1(a)]. The THUNDER actuators (THin layer composite UNimorph piezoelectric Driver and sEnsoR), developed by the NASA Langley Research Center and produced by FACE International Corporation, deform out of plane under an excitation voltage. THUNDERs are characterized by many advantages such as high displacement, acceptable load capacity and small size. Typically, without any loading, the present actuator (THUNDER-11R) with a physical dimension of $76.2\times2.54\times0.74$ mm can vibrate at a maximum displacement of about 2 mm and a frequency up to 2 kHz.[24] The actuators were installed in a cantilever manner to create the maximum perturbation displacement in the lateral direction and thus the best control performance under the same excitation condition.[25] The actuators and the walls of the slot around the actuators were well lubricated to minimize the contact friction. A thin piece of Mylar membrane, with superior strength, good heat resistance and insulation, was pasted on the top of the actuators to make a smooth airfoil surface (Fig. 1). Driven by the actuators, this membrane will oscillate to create a perturbation on the airfoil surface.

A cylindrical miniature electret pressure transducer (151-01 series, Tibbetts Ind.), with a sensitivity of 15.8 mV/Pa and a frequency response up to 10 kHz, was used to measure p at the airfoil leading edge, which provides both the feedback signal and a measure of the control performance. The cylindrical pressure transducer, with a diameter of 2.6 mm and a length of 7 mm, was embedded at the midspan of the airfoil, 1 mm from the airfoil leading edge and 1 mm below the $x-z$ plane [Fig. 1(a)], where the intensity of p was relative high.[1] The origin of the coordinate system, shown in Fig. 1(a), was defined at the cylinder center, with the x, y, and z along the streamwise, transverse, and spanwise directions, respectively. The two actuators were symmetrically located to the pressure transducer in the z direction [Fig. 1(a)]. The distance between the sensing element, i.e., the front end of the pressure transducer, and the cantilevered end of each actuator was 6, 5, and 4 mm in the x, y, and z directions, respectively.

As the pressure transducer and the actuators were very close to each other, it is crucial to ensure the output of the pressure transducer would not be affected by the disturbance generated by the actuators. A series of tests were carried out with the upstream cylinder removed. Under the same experimental conditions as used for present experiments, the actuators were excited by a sine wave of different combinations of the excitation frequency (f_e) and voltage (V_e) from a signal generator. The fluctuating flow pressure (p) and the perturbation displacement (Y_p) were simultaneously measured using the pressure transducer and the laser vibrometer, and then digitized for analysis. The number of the sampled points and the sampling time for each record were 20 000 and 10 s, respectively. The tests were divided into two parts. In the first part, V_e was fixed at 80 V and f_e was set at 30, 80, 160, 220, and 300 Hz, respectively. In the second part, f_e was fixed at 220 Hz and V_e was 10, 53, 80, 100, and 120 V, respectively. Note that the f_e/V_e pair included 220 Hz/80 and 220 Hz/53 V, which were the working frequencies and voltages to be used in the present control schemes. The root mean square (rms) value of p and Y_p, i.e., p_{rms} and $Y_{p,\mathrm{rms}}$, under different f_e and V_e are listed in Table I. It is evident that p_{rms} is almost constant, irrespective of $Y_{p,\mathrm{rms}}$, indicating that although the actuators and the pressure transducer were close to each other, the outputs of the pressure transducer would not be influenced by the disturbance generated by the actuators.

TABLE I. Perturbation effect on fluctuating flow pressure with the upstream cylinder removed.

	Experiment part 1					Experiment part 2				
V_e (V)	80	80	80	80	80	10	53	100	140	180
f_e (Hz)	30	80	160	220	300	220	220	220	220	220
$Y_{p,\mathrm{rms}}$ (mm)	0.46	0.38	0.28	0.21	0.19	0.03	0.13	0.23	0.31	0.34
p_{rms} (Pa)	22.4	22.3	22.4	22.4	22.4	22.3	22.4	22.5	22.4	22.4

Two 5 μm tungsten wires were placed at $x/d=8$, $y/d=-1$, $z/d=0$ (hot wire 1 in Fig. 1) and $x/d=10$, $y/d=-1$, $z/d=-8$ (hot wire 2 in Fig. 1), respectively, to measure the fluctuating flow velocity. Hot wires 1 and 2 were used to provide the feedback signal (u_1) and measure the vortical flow velocity (u_2), respectively. The location of the hot wire 1 is important for the control performance. The vortical flow should not be affected by the BVI, given more than $0.5\lambda_\infty$ upstream from the airfoil leading edge,[26] where λ_∞ is the vortex wavelength, estimated to be about $3.2d$ under the present Re_d condition. Therefore, hot wire 1 needs to be placed at $x/d<10-1.6=8.4$ so that u_1 is able to provide the information on the upstream unperturbed vortical flow, without the contamination of the BVI noises, to warrant a good control performance. Furthermore, hot wire 1 was placed at $y/d=-1$ in order to minimize its possible disturbance on the downstream flow near the airfoil leading edge. The feedback signal p or u_1 was, after amplification, high-pass-filtered at a cutoff frequency of 200 Hz (or 0.18 if normalized by d and U_∞) and then sent to a digital signal processor (DSP) controller fitted with 16 bit AD and DA converter. The converted analog signal was filtered again using a band-pass filter with a frequency range from 200 to 500 Hz (or from 0.18 to 0.45 if normalized) before amplification by a dual channel piezodriver amplifier (Trek PZD 700). The processed signal was then used to activate the actuators. The use of the two filters for the feed-forward and feedback passages was to remove noises from turbulence and electronics. The controller was implemented using a real-time system, dSPACE, which provided functions such as rapid control prototyping, production code generation, and hardware-in-the-loop tests. A DSP with SIMULINK function of MATLAB and software (ControlDesk 2.0) was used to sample and

process the feedback signals. In addition, the perturbation displacement of the membrane on the top of the actuators was measured by a Polytec Series 3000 Dual Beam laser vibrometer. The streamwise and lateral fluctuating flow velocities near the airfoil leading edge were measured using a 5 μm tungsten X wire. The signals, be they used for monitoring or feedback purposes, were simultaneously conditioned and digitized using a 12 bit AD board at a sampling frequency of 3.5 kHz per channel. The duration of each record was about 20 s.

Both flow visualization and PIV measurements were conducted using Dantec standard PIV2100 system. Flow was seeded by smoke generated from Paraffin oil and was illuminated in the plane of mean shear by two new wave standard pulsed laser sources of a wavelength of 532 nm, each having a maximum energy output of 120 mJ. Digital particle images were taken using one charge coupled device camera (HiSense type 13, gain $\times 4$, single frame for flow visualization or double frames for PIV, 1280×1024 pixels). A Dantec FlowMap Processor (PIV2100 type) was used to synchronize image taking and illumination. A wide-angle lens was used so that each image covered an area of 133 mm $\times$ 105 mm of the flow field, i.e., $x/d \approx 0.35-13.65$ and $y/d \approx -5.25-5.25$ for both flow visualization and PIV measurements. The longitudinal and lateral image magnifications were identical, i.e., 0.10 mm/pixel. In the image processing, 32×32 rectangular interrogation areas were used. Each interrogation area included 32 pixels with 25% overlap with other areas in either the longitudinal or lateral direction. The ensuing in-plane velocity vector field consisted of 53×42 vectors. Spanwise vorticity component, ω_z, was approximately obtained based on particle velocities using a central difference scheme. The spatial resolution of the vorticity estimate depends on grid spacing, approximately 2.5 mm or $0.25d$. See Zhang *et al.*[27] for more details of the flow visualization and PIV measurement.

III. PARAMETER OPTIMIZATION OF CLOSED-LOOP CONTROLLER

Two control schemes were investigated, referred to as p-control and u-control, using feedback signals from p and u_1, respectively. Both control schemes aim at reducing p. This was achieved by manually tuning two parameters involved in the feedback controller, i.e., an amplitude gain coefficient (A_{Y_pm}) and a time shift (t_{Y_pm}) between the perturbation displacement Y_p and the feedback signal m (representing p or u_1) of a closed-loop controller. The tuning process is to determine an optimum combination of A_{Y_pm} and t_{Y_pm}, which makes the rms value, p_{rms}, of p the minimum. The optimization procedure is as follows. First, vary A_{Y_pm} by keeping $t_{Y_pm}=0$ s to find a A_{Y_pm}, yielding a minimum p_{rms}. Second, given A_{Y_pm}, vary t_{Y_pm} within a range from 0 to 0.005 s to determine t_{Y_pm}, under which p_{rms} reaches the smallest. The reason for choosing the duration of 0.005 s is due to the dominance of f_s(=220 Hz) in the signal responses. Thus, the optimum t_{Y_pm} can be determined for one complete cycle of the vortex shedding, i.e., $1/f_s$ ($\approx$0.005 s). The whole process is then repeated on the basis of the optimum A_{Y_pm} and t_{Y_pm} to arrive at the final optimal combination of $A_{Y_pm,\mathrm{opt}}$ and $t_{Y_pm,\mathrm{opt}}$ for the closed-loop controller.

Figures 2 and 3 show the variation of p with respect to A_{Y_pm} and t_{Y_pm} for the two control schemes, respectively. For p-control scheme, A_{Y_pp} was first adjusted with t_{Y_pp} fixed at 0 s [Fig. 2(a)]. Evidently, at $A_{Y_pp}=3$, $p_{\mathrm{rms}}/p_{\mathrm{rms,nc}}$ is the lowest, where $p_{\mathrm{rms,nc}}$ represents the rms value of p without control. The unperturbed case is given in Figs. 2 and 3 by $p_{\mathrm{rms}}/p_{\mathrm{rms,nc}}=1$ and $A_{Y_pp}=0$, as indicated by a dashed line. Then, t_{Y_pp} was varied within a vortex shedding cycle at $A_{Y_pp}=3$ [Fig. 2(b)]. At $t_{Y_pp}=0.001\,52$ s, $p_{\mathrm{rms}}/p_{\mathrm{rms,nc}}$ displays its minimum, a 30.2% fall, and reaches the maximum at $t_{Y_pp}=0.004\,02$ s, a 4% amplification, compared with the unperturbed case. This time delay, i.e., $0.004\,02-0.001\,52=0.0025$ s, corresponds roughly to one half of the period of the vortex shedding, suggesting an anti-phased relation between the two extreme cases. With t_{Y_pp} set at 0.001 52 s, A_{Y_pp} was retuned. The lowest $p_{\mathrm{rms}}/p_{\mathrm{rms,nc}}$ occurs again at $A_{Y_pp}=3$ [Fig. 2(c)], where $p_{\mathrm{rms}}/p_{\mathrm{rms,nc}}$ is reduced by 30%, almost the same as that using $A_{Y_pp}=3$ and $t_{Y_pp}=0.001\,52$ s in Fig. 2(b). Further iterations performed failed to improve the control performance appreciably, implying that the results were already converged in the first three iterations, i.e., $A_{Y_pp}=3$ and $t_{Y_pp}=0.001\,52$ s were the optimum parameters of p-control scheme. The same optimization procedures were followed for u-control (Fig. 3) and $A_{Y_pu_1}=1.5$ and $t_{Y_pu_1}=0.001\,77$ s were found to be the optimum parameters. The whole tuning process finally led to an optimal configuration for each control scheme with the following parameters: $A_{Y_pp}=3$, $t_{Y_pp}=0.001\,52$ s for p-control; and $A_{Y_pu_1}=1.5$, $t_{Y_pu_1}=0.001\,77$ s for u-control. Unless otherwise stated, these parameters have been used to obtain the results discussed hereinafter.

IV. CONTROL PERFORMANCE

Using the above-mentioned tuned controllers, each control scheme was individually assessed to evaluate the control performance in terms of reducing p. Figure 4 shows the typical time histories of the fluctuating pressure coefficient $C_p[=p/(1/2)\rho U_\infty^2]$, with and without control, where ρ is air density. Compared with the unperturbed case [Fig. 4(a)], the rms value of C_p deceases by 30% for p-control [Fig. 4(b)] and by 39% for u-control [Fig. 4(c)].

The p spectrum, fE_p [Fig. 5(a)], displays a pronounced peak (7.45) at $f_s^*(=f_s d/U_\infty=0.205)$ in the absence of control. The power spectrum weighted by frequency f indicates the energy distribution with respect to f. The peak is apparently due to the Kármán vortices generated by the upstream cylinder. Once p-control is deployed, the peak value of fE_p at f_s^* retreats to 4.44 (a reduction by 40%), suggesting the impairment in the energy of p [Fig. 5(b)]. Yet, u-control leads to an even better performance, resulting in a reduction by 56% [Fig. 5(c)]. A more accurate method to estimate the energy of p ($E_{p,\Delta f}$) associated with f_s^* is to integrate E_p over a -3 dB bandwidth about f_s^* and then is multiplied by p_{rms}.

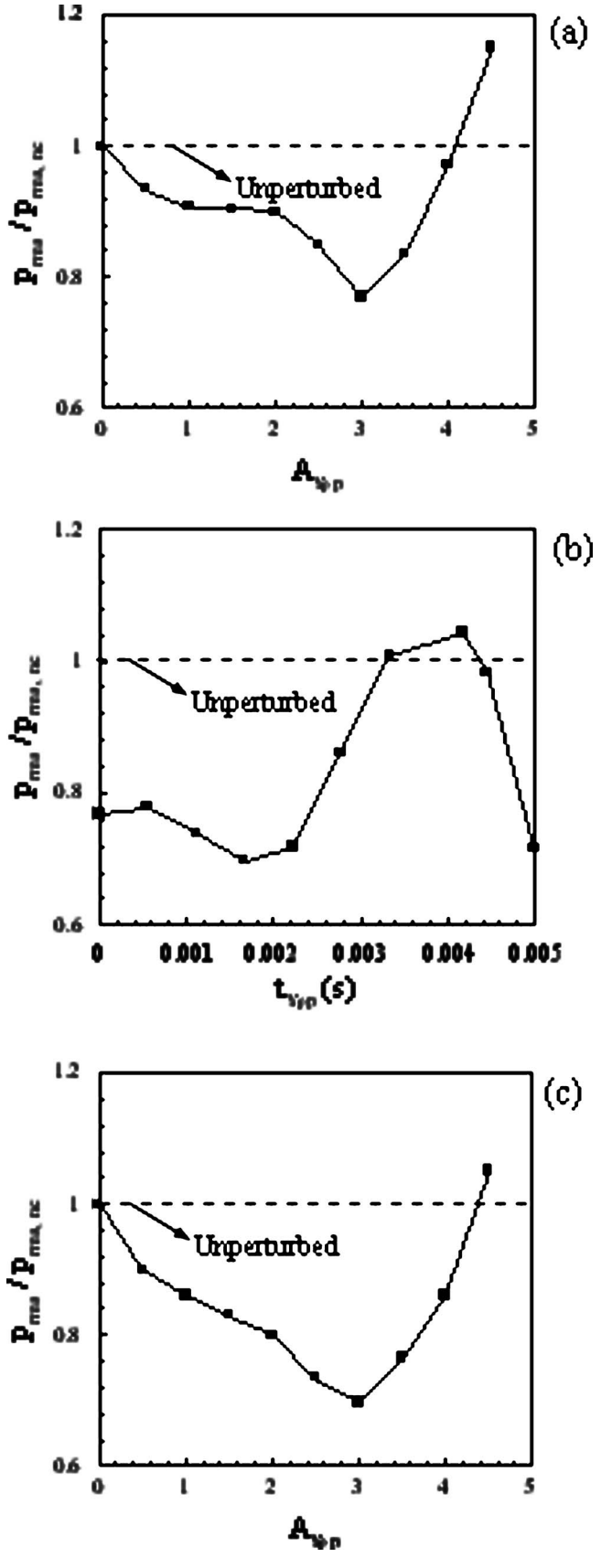

FIG. 2. Dependence of the root mean square value (p_{rms}) of the fluctuating flow pressure on the amplitude gain coefficient ($A_{Y_p p}$) or the time shift ($t_{Y_p p}$) between perturbation displacement (Y_p) and p under different control cases when p-control was deployed: (a) $t_{Y_p p}=0$ s; (b) $A_{Y_p p}=3$; and (c) $t_{Y_p p}=0.001\,52$ s.

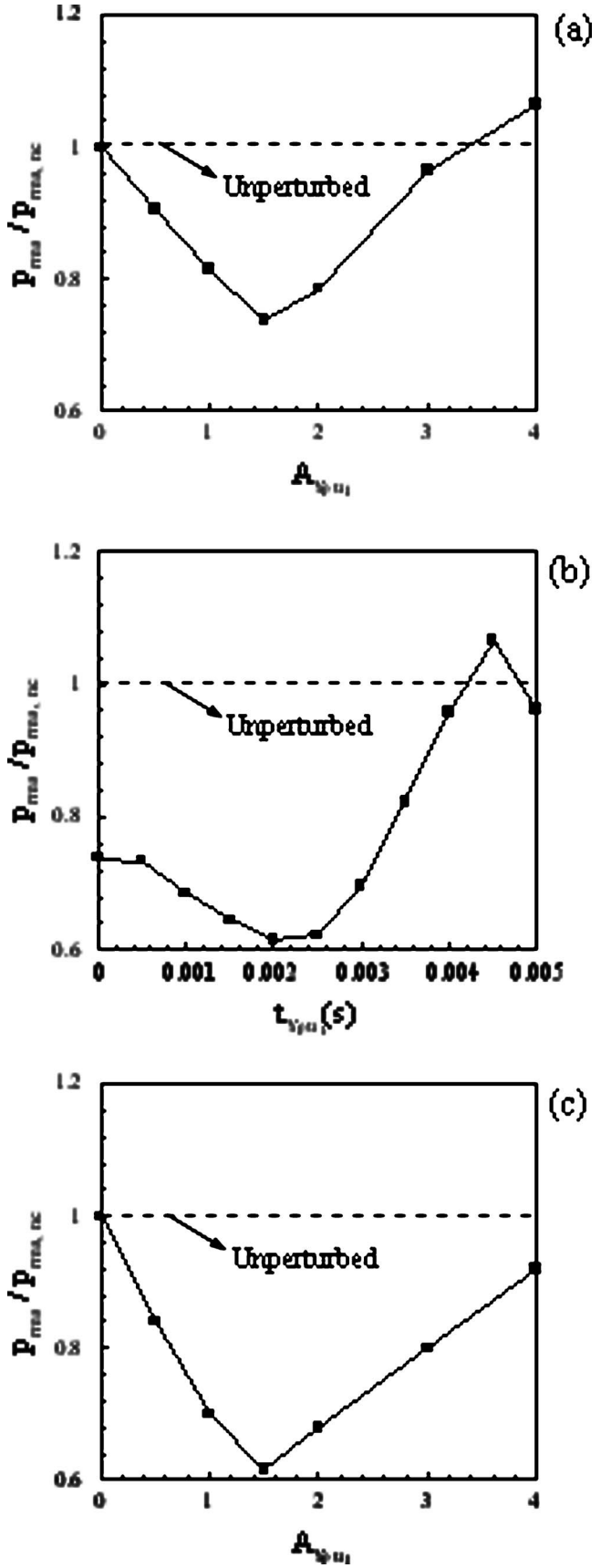

FIG. 3. Dependence of the root mean square value (p_{rms}) of the fluctuating flow pressure on the amplitude gain coefficient ($A_{Y_p u_1}$) or the time shift ($t_{Y_p p}$) between perturbation displacement (Y_p) and fluctuating flow velocity (u_1) under different control cases when $u_$control was deployed: (a) $t_{Y_p u_1}=0$ s; (b) $A_{Y_p u_1}=1.5$; and (c) $t_{Y_p u_1}=0.001\,77$ s.

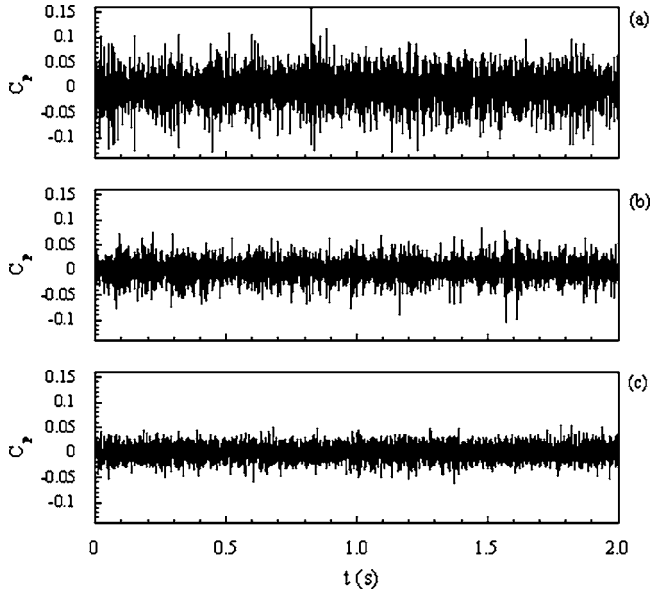

FIG. 4. Typical time histories of fluctuating pressure coefficient (C_p): (a) unperturbed; (b) p-control; and (c) u-control. The time origin is arbitrary.

Compared with the uncontrolled case, $E_{p,\Delta f}$ is effectively reduced by 52% for p-control and by 62% for u-control, seen in Table II.

Figure 6 shows the autocorrelation function, $R_{pp}(\tau)$, of p. The autocorrelation function of a signal α, i.e., $R_{\alpha\alpha}(\tau)$, is defined as

$$R_{\alpha\alpha}(\tau) = \lim_{T\to\infty} \frac{1}{T} \int_0^T \alpha(t)\alpha(t+\tau)dt, \tag{1}$$

where T(=20 s) and τ represent the sampling time and time delay, respectively.[28] Without control, $R_{pp}(\tau)$ [Fig. 6(a)] is essentially sinusoidal, displaying the same frequency as

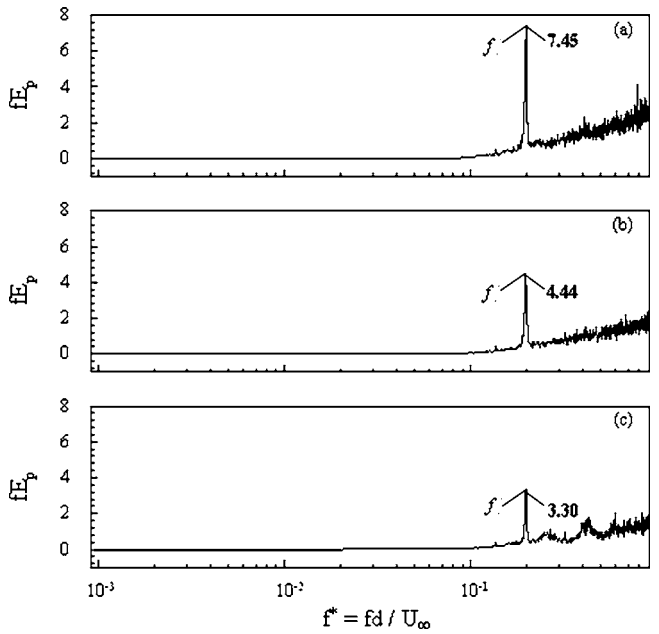

FIG. 5. Weighted power spectrum of the fluctuating flow pressure (p): (a) unperturbed; (b) p-control; (c) u-control.

TABLE II. Comparison in the energy reduction percentage of the fluctuating flow pressure (p) and the fluctuating streamwise flow velocity (u_2) at f_s^* between the two control schemes.

Energy	Control schemes	
	p-control	u-control
$E_{p,\Delta f}$	52%↓	62%↓
$E_{u_2,\Delta f}$	33%↓	42%↓

f_s=220 Hz, its amplitude reaching 0.4 (excluding those near τ=0) and decaying very slowly. The observation indicates that the unperturbed p is characterized by a strong periodicity associated with the oncoming Kármán vortices. With the control activated, however, $R_{pp}(\tau)$ [Figs. 6(b) and 6(c)] is significantly less periodical, with its amplitude decreased by roughly 50% in both cases. This loss in both the periodicity and the strength of $R_{pp}(\tau)$ shows the destructive effect of the perturbation on p.

The results demonstrate unequivocally the effectiveness of the present control technique on suppressing p and thus the BVI noise. Further, u-control is superior to p-control. It should be mentioned that the control voltage V_p required is approximately 80 and 53 V for p-control and u-control, respectively. The input energy E to the actuators may be approximately given by $E=2\pi f_s C V_p^2$,[29] where $C(\approx 4.16 \times 10^{-9}$ F) represents the capacitance of the actuator. E is about 0.037 and 0.016 J for p-control and u-control, respectively. It may be concluded that u-control outperforms p-control despite less actuation energy.

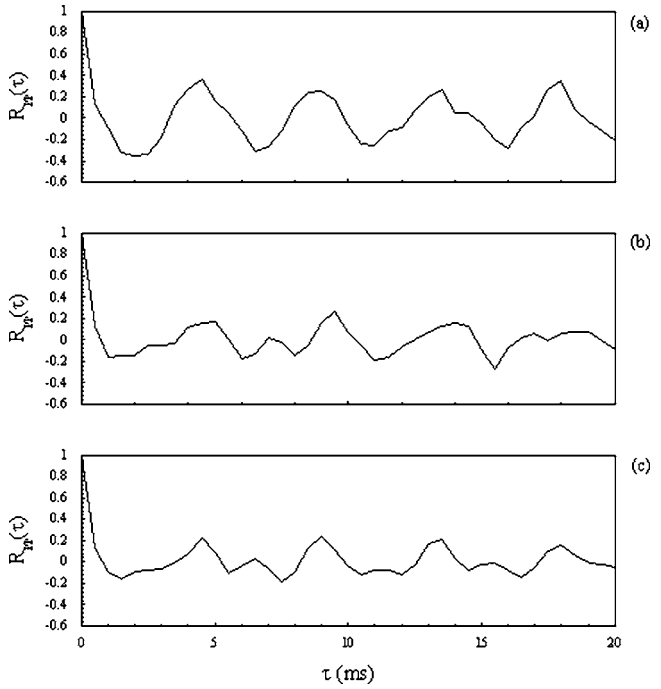

FIG. 6. The p-autocorrelation function $R_{pp}(\tau)$: (a) unperturbed; (b) p-control; and (c) u-control.

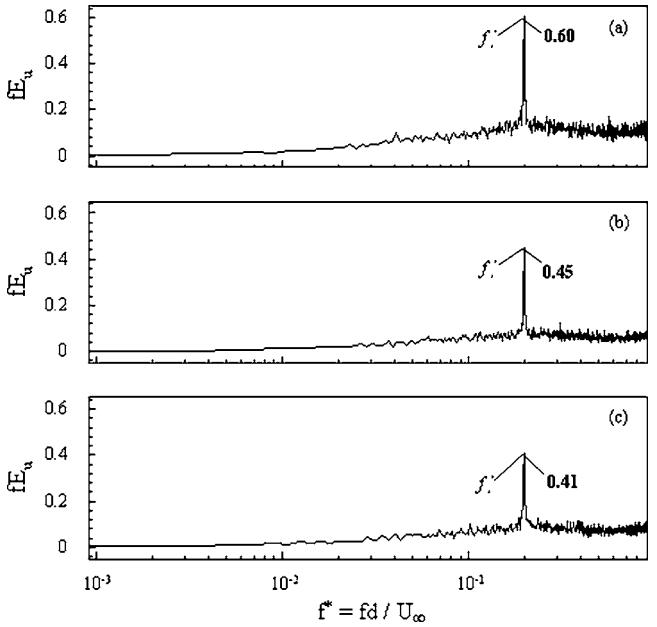

FIG. 7. Weighted power spectrum of the fluctuating flow velocity (u_2): (a) unperturbed; (b) p-control; and (c) u-control.

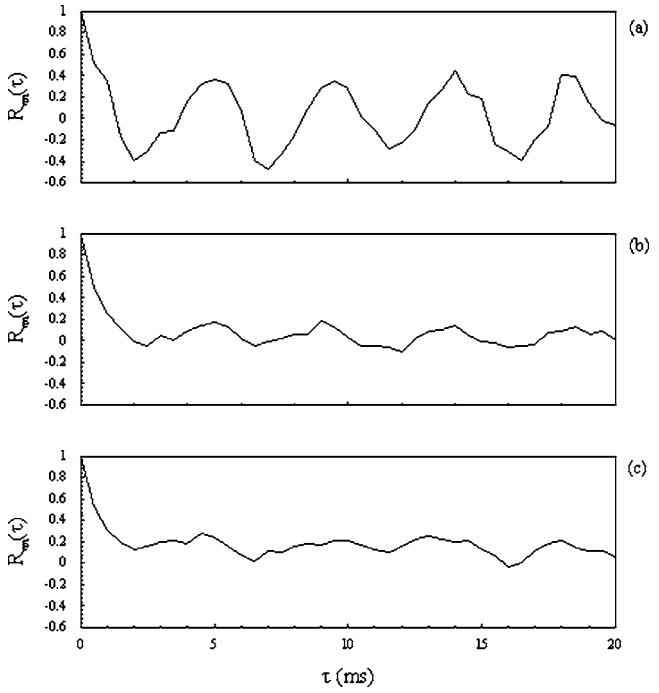

FIG. 8. The u_2-autocorrelation function $R_{uu}(\tau)$: (a) unperturbed; (b) p-control; and (c) u-control.

V. DISCUSSIONS

A. Perturbed oncoming vortical flow

It is of relevance to examine how the oncoming vortical flow responds to the control in order to improve our understanding of the underlying physics. Note that hot wire 2 was placed at $x/d=10$ and $y/d=-1$, close to the airfoil leading edge, where intensive vortex-airfoil interactions occur.[26] Figure 7 shows the weighted power spectra, i.e., fE_{u_2}, of u_2 with and without the closed-loop control. Compared with the unperturbed case [Fig. 7(a)], the peak in fE_{u_2} at f_s^* retreats by 25% and 32% for p-control [Fig. 7(b)] and u-control [Fig. 7(c)], respectively. The energy of u_2 around f_s^*, i.e., $E_{u_2,\Delta f}$, calculated similarly to $E_{p,\Delta f}$, exhibits a reduction by 33% for p-control and by 42% for u-control (Table II), suggesting a substantial impairment in the oncoming vortical structures. As a matter of fact, both the periodicity and the vortical structure strength have been attenuated once p- or u-control is introduced, as suggested by the u_2-autocorrelation function $R_{uu}(\tau)$ (Fig. 8). The difference in the reduction percentage between p- and u-control further indicates the superiority of u-control to p-control.

The control does not simply influence the oncoming flow locally. Figures 9 and 10 present typical flow visualization photos and the PIV-measured iso-contours of spanwise vorticity, $\omega_z^*=\omega_z d/U_\infty$, respectively. Once hitting the airfoil leading edge, the oncoming Kármán vortices are rapidly distorted into elongated elliptical structures with their major axes parallel to the mean flow. Gursul and Rockwell[26] attributed this deformation to the strain field around the airfoil leading edge. As shown in Figs. 9(b), 9(c), 10(b), and 10(c), the vorticity concentration region of the stretched vortices appears thinner, especially below the airfoil leading edge, which is near the perturbed surface, suggesting a reduced vortex strength. In fact, the averaged maximum spanwise vorticity ($\overline{\omega}_{z\max}^*$) and circulation ($\overline{\Gamma}$), estimated based on 25 PIV images, measured below the airfoil leading edge decrease by 21% and 31% for p-control, respectively, and by 28% and 40% for u-control, respectively, when compared with the unperturbed case. Each circulation Γ around a vortex is estimated by numerical integration $\Gamma^*=\Gamma/U_\infty d=\Sigma_{i,j}(\omega_z^*)_{ij}\Delta A/d^2$,[30] where $(\omega_z^*)_{ij}$ is spanwise vorticity over area $\Delta A=\Delta x\Delta y$, Δx and Δy being the integral step along x and y directions, respectively. The magnitude $|\omega_z^*|=0.1$, about 7% of $|\omega_{z\max}^*|$, has been used as the cutoff level, which is the same as the level used by Cantwell and Coles.[30]

Figure 11 shows the lateral distribution of fluctuating streamwise flow velocity $u_{\rm rms}$, i.e., the rms of u, measured at $x/d=10$ and $y/d=-0.5$, -1, -1.5, and -2 using a hot wire. The measured $u_{\rm rms}$ is normalized by its uncontrolled counterpart, i.e., $u_{\rm rms,nc}$. Under both control schemes, $u_{\rm rms}$ drops considerably, conforming to the observation from the spectra (Fig. 7). The maximum reduction occurs near the airfoil leading edge, where $u_{\rm rms}/u_{\rm rms,nc}$ is 0.79 and 0.82 for u-control and p-control, respectively; the reduction is still appreciable, $u_{\rm rms}/u_{\rm rms,nc}\approx 0.95$, even at $y/d=-2$. The observation is internally consistent with flow visualization and PIV results. It may be concluded that the surface perturbation near the airfoil leading edge has made a pronounced modification on the oncoming flow field.

Strictly speaking, the BVI noise should be really estimated by pressure distributions along the front of the airfoil, not just pressure at a point. However, the measurement of the pressure distribution around the airfoil leading edge is very difficult, if not impossible, because a large number of sensors are required. Under the bombardment of the oncoming vortices, the rise of the fluctuating flow pressure induced by the distortion of the vortices near the airfoil leading edge should

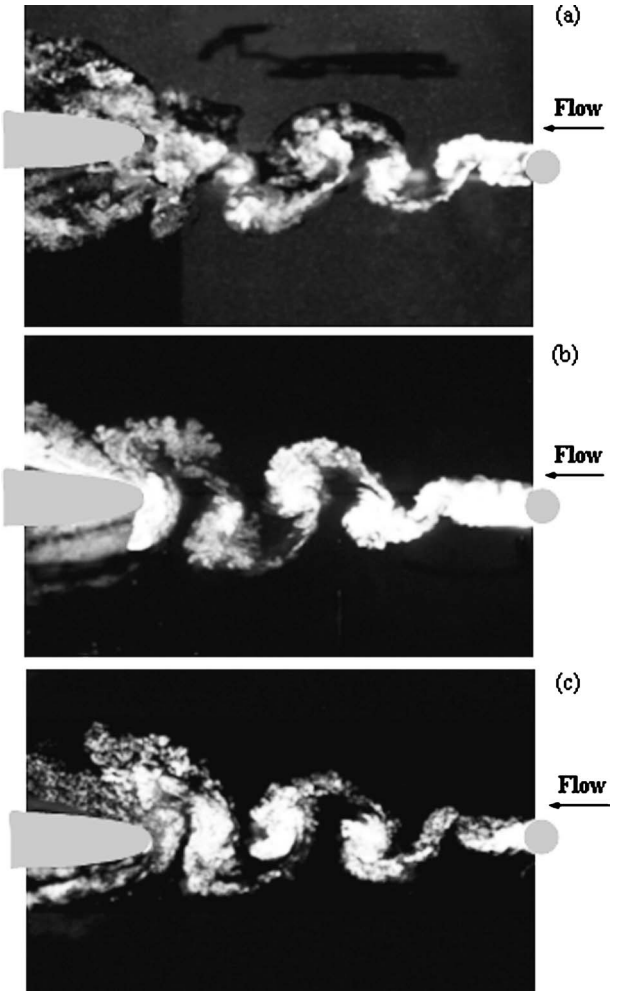

FIG. 9. Typical flow visualization photos: (a) unperturbed; (b) p-control; and (c) u-control. $\mathrm{Re}_d = 7300$.

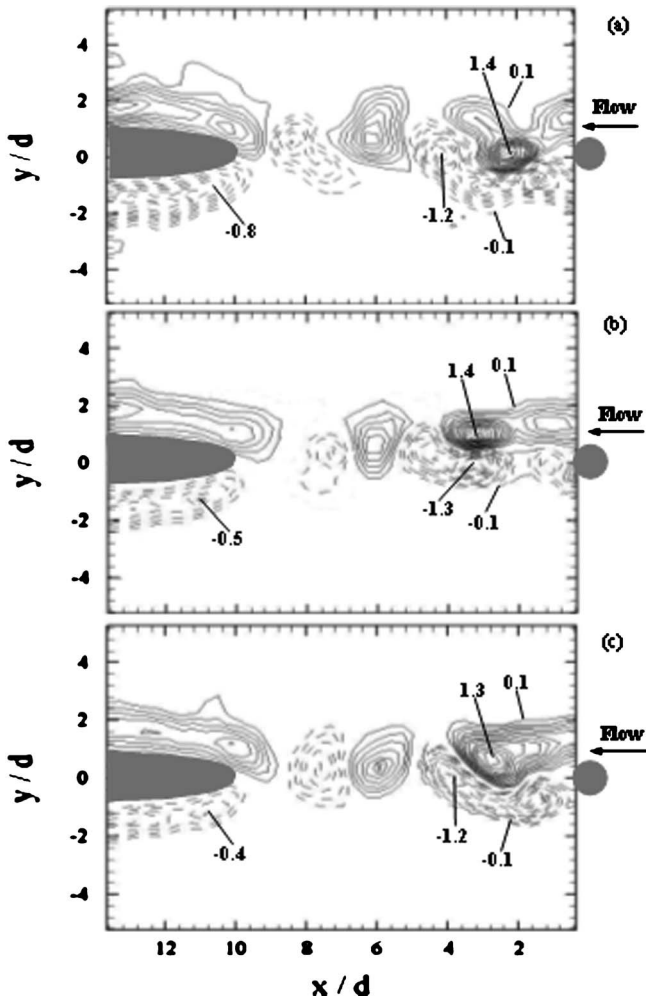

FIG. 10. Typical PIV-measured iso-contours of spanwise vorticity $\omega_z^* = \omega_z d / U_\infty$: (a) unperturbed; (b) p-control; and (c) u-control. $\mathrm{Re}_d = 7300$. The contour increment is 0.1.

spread a certain spatial extent and be reasonably continuous, not a spike. This is supported by instantaneous flow visualization and PIV results (Figs. 9 and 10), which show that the interaction between the airfoil surface and incoming large-scale vortices occurs over almost the entire leading edge of the airfoil. This interaction determines to a great extent the fluctuating flow pressure p. Therefore, p measured at one point should be able to provide a good indication of the average level of the pressure distribution over the airfoil leading edge.

B. Perturbed vortex-airfoil interactions

Insight may be gained into the perturbation vortex-airfoil interaction process by examining the spectral phases between simultaneously measured u_1, u_2, p, and Y_p with and without control, i.e., $\Phi_{\alpha_1\alpha_2} \equiv \tan^{-1}(Q_{\alpha_1\alpha_2}/Co_{\alpha_1\alpha_2})$, where α_1 and α_2 represent two signals and $Co_{\alpha_1\alpha_2}$ and $Q_{\alpha_1\alpha_2}$ stand for the co-spectrum and quadrature spectrum, respectively. The co-spectrum and quadrature spectrum, i.e., $Co_{\alpha_1\alpha_2}$ and $Q_{\alpha_1\alpha_2}$, are defined by

$$Co_{\alpha_1\alpha_2}(f) = 2\int_{-\infty}^{\infty} R_{\alpha_1\alpha_2}(\tau)\cos 2\pi f\tau d\tau, \tag{2}$$

$$Q_{\alpha_1\alpha_2}(f) = 2\int_{-\infty}^{\infty} R_{\alpha_1\alpha_2}(\tau)\sin 2\pi f\tau d\tau \tag{3}$$

(Ref. 28), where τ and $R_{\alpha_1\alpha_2}$ are time delay and cross-correlation function between α_1 and α_2, respectively. $R_{\alpha_1\alpha_2}$ is defined by

$$R_{\alpha_1\alpha_2}(\tau) = \lim_{T\to\infty} \frac{1}{T}\int_0^T \alpha_1(t)\alpha_2(t+\tau)dt \tag{4}$$

(Ref. 28). The spectra were computed using a fast Fourier transform method.[31] As an example, Fig. 12 shows the effect of the u-control scheme on the spectral phase $\phi_{u_2u_1}$ between u_2 and u_1, where u_1 and u_2 were measured using hot wire 1 at $x/d=8$ and $y/d=-1$ and hot wire 2 at $x/d=10$ and $y/d=-1$. Without perturbation, $\phi_{u_2u_1}$ [Fig. 12(a)] and also ϕ_{pu_1} at f_s^* are approximately zero, suggesting that the unperturbed p, u_1, and u_2 are all in-phased at the dominant vortex frequency. In the wake of a circular cylinder, the Kármán vortex wavelength is about $4.3d$ for the present Re. Since the hot wires 1 and 2 were longitudinally separated by $2d$ (Sec. II), about one-half of the wavelength, their measured u_1 and u_2 should be antiphased at f_s^* in the absence of the airfoil,

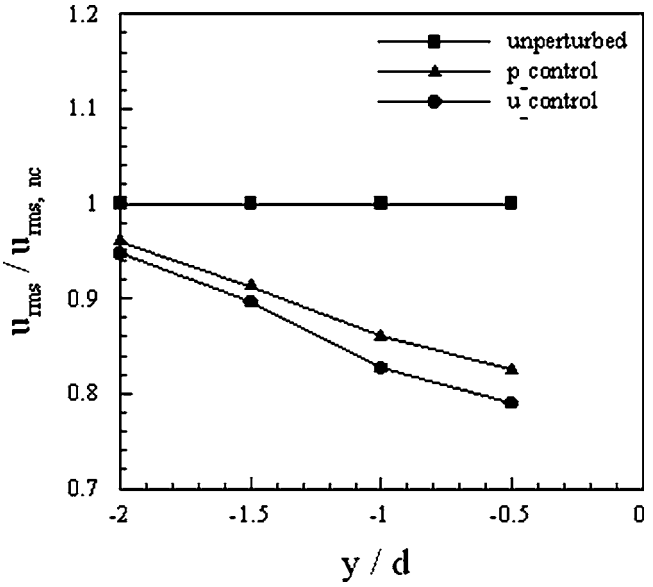

FIG. 11. The lateral variation of the rms value of fluctuating flow velocity (u_2) with and without control ($x/d=10$).

which may be inferred from Fig. 9(a) in Zhou *et al.*[23] The present observation of the in-phased u_1 and u_2 at f_s^* suggests that the incident vortical flow has been significantly modified as a result of the vortex-airfoil interaction.

Under u-control, $\phi_{u_2u_1}$ at f_s^* is now about -0.7 [Fig. 12(b)]. However, ϕ_{pu_1} at f_s^* remains zero. As mentioned earlier, the measurement location of u_1 was carefully selected so that u_1 would not be influenced by the vortex-airfoil interaction. It may be inferred that it is the perturbation that has modified the phase of u_2 with respect to u_1 at f_s^*. In the u-control, the time shift $t_{Y_pu_1}$ between Y_p and u_1 was set to be 0.001 77 s, roughly corresponding to a phase shift $\phi_{Y_pu_1}=2.44$ ($\approx 0.001\ 77\ \text{s}\times 2\pi\times f_s$, $f_s=220$ Hz) at f_s^*. Noting $\phi_{u_2u_1}=-0.7$ at f_s^*, the spectral phase $\phi_{Y_pu_2}$ between Y_p and u_2 at f_s^* should be approximately π or antiphased. Similarly, $\phi_{Y_pu_2}$ at f_s^* should also be approximately $-\pi$ under the p-control scheme. This is indeed confirmed by the result of $\phi_{Y_pu_2}$, where $\phi_{Y_pu_2}$ at f_s^* is close to $-\pi$ for both control schemes, indicating that the measurements are internally consistent.

In an investigation to control the flow-induced vibration on a laterally oscillating square cylinder, Cheng *et al.*[18] found that the spectral phase between the lateral structural displacement Y and the streamwise fluctuating flow velocity u was approximately equivalent to that between the lateral cylinder oscillating velocity, $\dot{Y}$, and the lateral flow velocity v. The present case differs from theirs in that the airfoil leading edge is bombarded by incident vortices, instead of shedding vortices. Therefore, one experiment was carried out to investigate the relationship between flow and perturbation force. One movable X wire was used to measure the lateral fluctuating flow velocity v near the lower side of the airfoil leading edge, simultaneously with the airfoil surface perturbation velocity $\dot{Y}_p$ measured using a laser vibrometer. The spectral phase $\phi_{\dot{Y}_pv}$ between v and $\dot{Y}_p$ at f_s^* (not shown) was

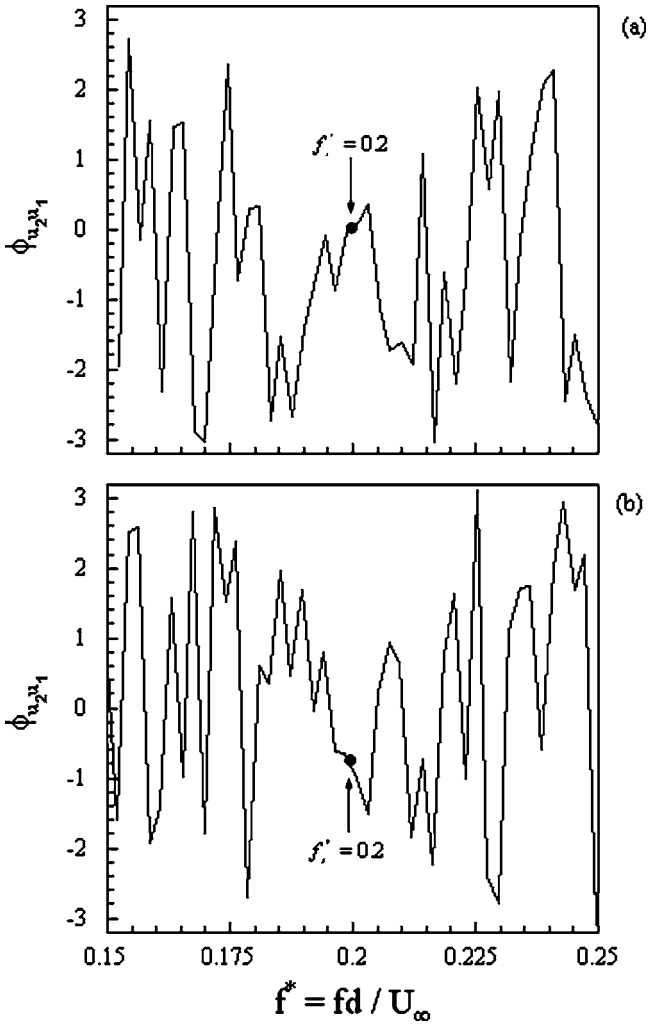

FIG. 12. Spectral phase $\phi_{u_2u_1}$ between the fluctuating flow velocity (u_2) at $x/d=10$ and $y/d=-1$ and the fluctuating flow velocity (u_1) at $x/d=8$ and $y/d=-1$: (a) unperturbed and (b) u-control.

close to $-\pi$ for both p- and u-control schemes when the X wire was moved over $x/d\approx 9.8-11$ and $y/d\approx -1.25$ to -0.7, which was near the perturbed surface ($x/d=10.7$ and $y/d=-0.5$). The airfoil surface perturbation velocity $\dot{Y}_p$ is approximately in the lateral direction since the normal direction of the perturbation surface is about 87° with respect to the longitudinal direction [Fig. 1(a)]. Note that, with the two actuators activated simultaneously, $\dot{Y}_p$ is uniform along the spanwise direction. Considering the two dimensionality of flow and perturbation, $\phi_{\dot{Y}_pv}=-\pi$ at f_s^* should hold along the spanwise direction. This phase relationship means the opposite or collided movements between the local airfoil surface perturbation and the local vortical flow, which exerts a significant influence on the whole unsteady vortex structure and subsequently weakens the vortex strength. This vortex strength reduction, presently by 31% (Figs. 9 and 10), will in turn cause a weakened fluctuating flow pressure near the airfoil leading edge and subsequently its induced BVI noise because of their close link.[4,15]

One may surmise that the vortex-airfoil interaction could modify the spectral phase ϕ_{uv} between the streamwise and

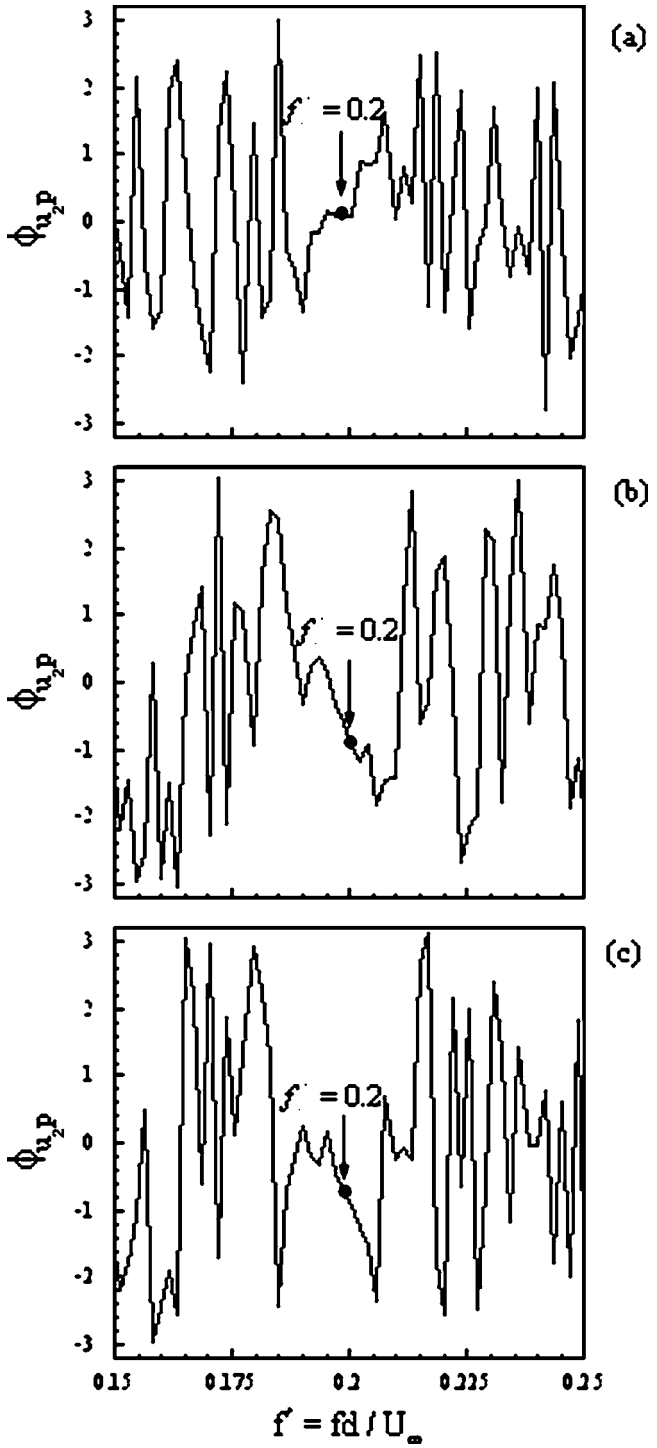

FIG. 13. Spectral phase ϕ_{u_2p} between the fluctuating flow velocity (u_2) and the fluctuating flow pressure signal (p): (a) unperturbed; (b) perturbed under p-control; and (c) perturbed under u-control.

lateral fluctuating flow velocity, i.e., u and v. To clarify this point, one test was done, with one X wire used to measure simultaneously u and v at the location where hot wire 2 was placed, i.e., $x/d=10$ and $y/d=-1$. Measurements were conducted with and without control. Thus obtained ϕ_{uv} at f_s^* was approximately $-\pi/2$ in both cases (not shown), indicating that the phase between u and v is not affected by control.

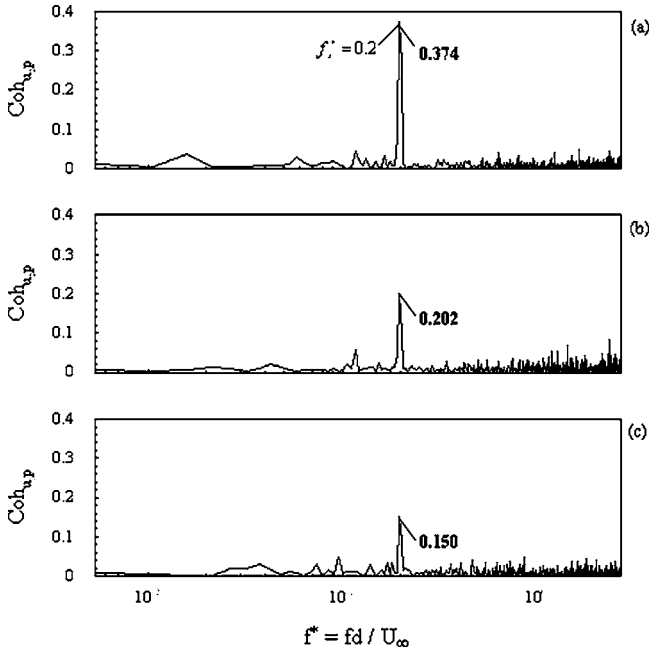

FIG. 14. Spectral coherence Coh_{u_2p} between the fluctuating flow velocity (u_2) and the fluctuating flow pressure signal (p): (a) unperturbed; (b) p-control; and (c) u-control.

Therefore, the equivalence between Y_p-u and $\dot{Y}_p-v$ still holds presently in terms of the phase relationship.

As previously discussed, the unperturbed u_2 and p should be in-phased, i.e., $\phi_{u_2p}=0$, at f_s^*. This is indeed verified in Fig. 13(a). Once the p-control is applied, ϕ_{u_2p} may be derived by subtracting $\phi_{Y_pu_2}$ from the spectral phase ϕ_{Y_pp}. Recall that the time shift t_{Y_pp} under the p-control is 0.001 52 s. Then ϕ_{Y_pp} at f_s^* can be approximately calculated by $\phi_{Y_pp}=t_{Y_pp}\times 2\pi\times f_s\approx 2.1$. Thus $\phi_{u_2p}=\phi_{Y_pp}-\phi_{Y_pu_2}=2.1-(-\pi)$ or $-2\pi+2.1-(-\pi)\approx -1$. On the other hand, for the u-control, ϕ_{u_2p} at f_s^* is the difference between $\phi_{u_2u_1}(=-0.7)$ and ϕ_{pu_1} at $f_s^*(=0)$. The previous analysis is indeed confirmed by ϕ_{u_2p} at f_s^* calculated from the simultaneously measured u_2 and p [Figs. 13(b) and 13(c)].

The phase shift at f_s^* between u_2 and p may reflect the vortex-airfoil interaction because u_2 contains the information on the distortion of the incident vortical flow near the airfoil leading edge, which is responsible for the generation of the fluctuating flow pressure, and subsequent the BVI noise. In the absence of perturbation, u_2 synchronized with p always over a range of frequencies about f_s^* [Fig. 13(a)]. Once the control is introduced, ϕ_{u_2p} between u_2 and p at f_s^* are changed [Figs. 13(b) and 13(c)], implying an altered vortex-airfoil interaction. The spectral coherence $\mathrm{Coh}_{u_2p}[=(\mathrm{Co}_{u_2p}^2+Q_{u_2p}^2)/E_{u_2}E_p)]$ provides a measure of the degree of correlation between the Fourier components of u_2 and p. The peak in Coh_{u_2p} at f_s^* reaches about 0.37 without perturbation [Fig. 14(a)], suggesting a strong correlation between the oncoming vortices and airfoil. However, this peak recedes by 46% for the p-control [Fig. 14(b)] and by 60% for the u-control [Fig. 14(c)], that is, the oncoming vortices and the fluctuating flow pressure on the airfoil become weakly correlated.

Based on the above-mentioned analyses, an interpretation for the impaired p is now proposed. The impulsive fluctuating flow pressure and hence the BVI noise originate from the drastic distortion of the incident vortices, which is created by the vigorous interaction between vortices and airfoil leading edge. As demonstrated earlier, the closed-loop controlled surface perturbation $\dot{Y}_p$ and v associated with the incoming vortices are antiphased. This "collision" may act to reduce substantially the vortex strength,[32] and hence the fluctuating flow pressure on the airfoil leading edge or the BVI noise.

Using the u-control scheme, the feedback signal is taken from the vortical flow upstream of the airfoil, which is the excitation source. Therefore, the effect of the control action is to modify directly the flow excitation and subsequently p. On the other hand, the p-control scheme uses p, i.e., the passive response of the vortex-airfoil interaction, as the feedback signal, instead of the excitation source. Consequently, the control performance is less effective than the u-control scheme, even though the input energy is nearly 2.3 times that used in the u-control scheme.

VI. CONCLUSIONS

Closed-loop control of the vortex-airfoil interaction has been experimentally investigated with a view to suppress the BVI noise. Two control schemes were investigated and compared, leading to the following conclusions.

(1) The proposed closed-loop control technique is effective to suppress the pressure rise, generated from vortex-airfoil interactions, at the leading edge of the airfoil. The choice of the feedback signal may have considerable effect on the control performance. The u-control scheme reduced the rms value of p by 39% whereas p-control scheme reduced that by 30%. The difference is ascribed to the fact that the u signal is linked to the excitation source of the noise, whereas the p signal reflects the passive response of the vortex-airfoil interaction. The observation points to a crucial role of the feedback signal played in the closed-loop control of the BVI noise.

(2) In a successful control, an antiphased relationship occurs between the controlled perturbation velocity and the lateral fluctuating flow velocity associated with incident vortices. This antiphase relationship significantly impairs the oncoming vortex strength and vortex-airfoil interaction, resulting in a remarkable reduction in the fluctuating flow pressure around the airfoil leading edge and subsequent the BVI noise.

ACKNOWLEDGMENTS

The authors wish to acknowledge support given to them by the Research Grants Council of HKSAR through Grants No. PolyU 5294/03E and No. PolyU 1/02C. The second author (L.C.) wishes to acknowledge the support from a special fund for recently promoted Chair Professors given by The Hong Kong Polytechnic University.

[1] S. Ziada and D. Rockwell, "Vortex-leading-edge interaction," J. Fluid Mech. **118**, 79 (1982).
[2] E. R. Booth, Jr., and J. C. Yu, "Two-dimensional blade-vortex flow visualization investigation," AIAA J. **24**, 1468 (1986).
[3] J. C. Hardin and S. L. Lamkin, "Concepts for reduction of blade/vortex interaction noise," J. Aircr. **24**, 120 (1987).
[4] D. Rockwell, "Vortex-body interactions," Annu. Rev. Fluid Mech. **30**, 199 (1998).
[5] M. S. Howe, *Theory of Vortex Sound* (Cambridge University Press, San Diego, 2003).
[6] M. V. Lowson, "Progress towards quieter civil helicopters," Aeronaut. J. **96**, 209 (1992).
[7] A. Brocklehurst and A. C. Pike, *Reduction of BVI Noise Using a Vane Tip* (American Helicopter Society, San Francisco, CA, 1994).
[8] W. S. Hindson and R. T. N. Chen, "Operational tests of noise abatement for rotorcraft using differential GPS for guidance," J. Am. Helicopter Soc. **43**, 352 (1998).
[9] F. H. Schmitz, G. Gopalan, and B. Wel -C. Sim, "Flight-path management/control methodology to reduce helicopter blade-vortex interaction noise," J. Aircr. **39**, 193 (2002).
[10] T. F. Brooks, E. R. Booth, Jr., and D. D. Boyd, Jr., "Analysis of a higher harmonic control test to reduce blade vortex interaction noise," J. Aircr. **31**, 1341 (1994).
[11] S. A. Jackin, A. Blaas, D. Teves, and R. Kube, "Reduction of helicopter BVI noise, vibration, and power consumption through individual blade control," 51st Annual Forum of the American Helicopter Society, Fort Worth, TX, 1995.
[12] P. C. Chen, J. D. Baeder, R. A. D. Evans, and J. Niemczuk, "Blade-vortex interaction noise reduction with active twist smart rotor technology," Smart Mater. Struct. **10**, 77 (2001).
[13] F. K. Straub, D. K. Kennedy, D. B. Domzalski, A. A. Hassan, H. Ngo, V. Anand, and T. Birchette, "Smart material-actuated rotor technology-SMART," J. Intell. Mater. Syst. Struct. **15**, 249 (2004).
[14] C. R. Kaykayoğlu, "Active control of a mixing layer by upstream influence from an oscillating edge," J. Fluids Struct. **3**, 1 (1989).
[15] S. Lee, "Reduction of blade-vortex interaction noise through porous leading edge," AIAA J. **32**, 480 (1994).
[16] K. B. Ariyur and M. Krstić, "Feedback attenuation and adaptive cancellation of blade vortex interaction on a helicopter blade element," IEEE Trans. Control Syst. Technol. **7**, 596 (1999).
[17] R. Swaminathan, J. V. R. Prasad, and L. N. Sankar, "Active control of blade-vortex interactions using a neuro-fuzzy controller," in Proceeding of the Third European Conference on Smart Structures Materials, Lyon, France, 1996.
[18] L. Cheng, Y. Zhou, and M. M. Zhang, "Perturbed interaction between vortex shedding and induced vibration," J. Fluids Struct. **17**, 887 (2003).
[19] M. M. Zhang, L. Cheng, and Y. Zhou, "Closed-loop-controlled vortex shedding from a flexibly supported square cylinder under different schemes," Phys. Fluids **16**, 1439 (2004).
[20] M. C. Wilder and D. P. Telionis, "Parallel blade-vortex interaction," J. Fluids Struct. **12**, 801 (1998).
[21] M. Michard, M. C. Jacob, and N. Grosjean, "An experimental characterization of the flow past an airfoil in the wake of a circular rod," in Proceedings of ASME FEDSM'02 ASME 2002 Fluids Engineering Division Summer Meeting, Montreal, Quebec, Canada, 14–18 July 2002.
[22] W. S. Kamiński and A. P. Szumowski, "Acoustic effects of parallel vortex-airfoil interaction," J. Sound Vib. **183**, 209 (1995).
[23] Y. Zhou, H. J. Zhang, and M. W. Yiu, "The turbulent wake of two side-by-side circular cylinders," J. Fluid Mech. **458**, 303 (2002).
[24] B. M. Copeland, J. D. Buckley, R. G. Bryant, R. L. Fox, and R. F. Hellbaum, "THUNDER—an ultra-high displacement piezoelectric actuator," NASA Langley Research Center, Hampton, VA, 23681-0001, 1999.
[25] J. P. Marouze and L. Cheng, "A feasibility study of active vibration isolation using THUNDER actuators," Smart Mater. Struct. **11**, 854 (2002).
[26] I. Gursul and D. Rockwell, "Vortex street impinging upon an elliptical leading edge," J. Fluid Mech. **211**, 211 (1990).
[27] M. M. Zhang, Y. Zhou, and L. Cheng, "Spring-supported cylinder wake control," AIAA J. **41**, 1500 (2003).
[28] A. M. Yaglom, *Correlation Theory of Stationary and Related Random Functions* (Springer, New York, 1987).
[29] L. K. Baxter, *Capacitive Sensors: Design and Applications* (IEEE, New York, 1997).

[30]B. J. Cantwell and D. Coles, "An experimental study of entrainment and transport in the turbulent near wake of a circular cylinder," J. Fluid Mech. **136**, 321 (1983).
[31]H. J. Zhang, Y. Zhou, and R. A. Antonia, "Longitudinal and spanwise structures in a turbulent wake," Phys. Fluids **11**, 2954 (2000).
[32]M. M. Zhang, L. Cheng, and Y. Zhou, "Closed-loop manipulation of vortex shedding from a fixed-supported square cylinder," Exp. Fluids **39**, 75 (2005).